Scholar Publishing Group
International Journal of Art Innovation and Development
https://doi.org/10.38007/IJAID.2022.030103
ISSN 2789-7192 Vol. 3, Issue 1: 28-44

Computer-assisted Tang Songcai Crafts Surface Nano Processing Technology

Bin Chen*

Fuzhou University of International Studies and Trade, Fuzhou, Fujian, China

**corresponding author*

Keywords: Computer Assist, Artificial Neural Network, Tang Sangcai, Nano Si3N4

Abstract: Tang Sancai is the first ceramic variety using cobalt blue color as a decorated system in China's ceramic system. It laid the foundation for this development and prosperity. With the development of social development, the application of computer technology is very wide. Tang Singer's crafts use computer production, can stimulate craftsmen' creative thinking, help design, reduce production costs, improve product quality, and obtain competitive advantages. The GRNN model is used to simulate the Si2N2O-Sialon ceramic superplastic extrusion process, and the strength and effect of extrusion deformation under different temperature and pressure and tension distribution during extrusion process are obtained. Studies have shown that the elongation of Si2N2O-Si3N4 ceramics at 1550 ℃ can reach 65%, and nano-Si2N2O-Sialon ceramics have better superplasticity.

1. Introduction

Tang tricolor is one of the components of the historical development process of Chinese ceramic technology. It has become the most representative craft products in the Tang Dynasty with its bright color and strong life atmosphere. Also because of its distinctive decorative art on the later generations, and even the contemporary society aesthetic decoration has a profound influence.

Silicon nitride is an ideal high temperature structure material, which is currently considered as one of the most promising materials in the field of high temperature in ceramics. It has the characteristics of high hardness and good wear resistance, so the complex parts are difficult to be processed forming. The excellent performance of nano-pottery materials has attracted great attention in the world. However, because it is difficult to control the growth of grain at high temperature, the preparation of high-performance nanoscale silicon nitride ceramics is one of the hot spots in the research field of silicon nitride ceramics. The preparation of nano-silicon nitride ceramics with good comprehensive performance not only meets the application of engineering field in the comprehensive performance, but also has good superplasticity, which can carry out superplastic forming, which is of great significance for the practical application of silicon nitride

ceramics.

In this paper, Si2N2O-Si3N4 and Si2N2O-Sialon nano-ceramics were prepared by liquid-phase sintering of amorphous nano-Si3N4 powder according to hot pressing sintering process. It studied the superplastic forming properties and forming laws of two ceramic materials by combining experimental research with finite element simulation.

2. Related Work

Today's world is being changed by computer digital technology, and traditional ceramic craftsmanship is also being changed by the influence of modern computer technology. Anitha R used a computer auxiliary method to automatically detect and diagnose cerebral tumors, and proposed brain tumor detection and segmentation methods based on random forest classifiers, which classified the brain image as normal or abnormal. He analyzed the proposed brain tumor detection and segmentation system from sensitivity, specificity, false positive rate, false negative, positive likelihood ratio, negative ratio, etc. [1]. Acharya V's research proposed an image processing technology for calculating the number of red blood cells. It is intended to check and process the blood smear image to support the red blood cell count and automatically identify the amount of normal and abnormal cells in the image. K-MedoIDS algorithm with robustness of external noise is used to extract WBC from the image [2]. The main goal of Bukhari N i was to develop oral activated cefotaxime sodium (CS) in the Eudragit S100 polymer using a pH sensitive nanocrynect. Oral administration of the water dispersion of the particles was allowed to fight against the control. Plasma concentration and pharmacokinetic parameters, within 6 hours after administration, are better to nanoparticles [3]. Daemei A B assumed that computer-aided design, experience, sketch, physical modeling, learning environment, and image and visual reference can be used as a powerful tool for stimulating creativity during architectural design. It tried to investigate which of these components have the greatest impact on improving students' creativity. The results showed that experience can significantly improve the creativity of students in the architectural design compared to other components [4]. Alanis introduced the results of the use of circulating neural network training algorithms based on extended Kalman filters and their applications in electricity price forecasts, which divided into two cases: one step in advance and N steps in advance. Finally, by using the European power system data, the pre-prediction of N step prediction is indicated of the applicability of the proposed prediction scheme [5]. RavicHandran V outlines a variety of neural networks, focusing on the network based on recruiting emerging devices. It has an advantage compared to pure complementary metal oxide semiconductor (CMOS). He introduced the general description of the neural network, then investigated the famous CMOS network, finally discussed the network implemented by emerging resentment devices, as well as the development of the motivation based on memoirers and the calculation potential of these networks [6]. Dc A is characterized to the glaze of Yellow Ye and Huanglue, and found that the Si / Al ratio of these samples is much higher than their body samples, which means that the silica raw material is intentionally added in the glaze [7]. Widerski A described how to use artificial neural networks to operate operational assessment of vehicles used in freight services. The basis of verifying the method was the experimental study conducted by a company that produces dairy products, working with transportation companies to provide products for the production process [8]. In the composite, Zhang L enhanced the dispersion and mechanical properties of Si3N4 by molecular dynamic simulation of hydrogen bond networks in composites [9]. These studies have certain guidance, but the study can be further improved.

3. Nano-ceramic Materials and Computer Auxiliary Technology Related Basic Theories

3.1. Silicon Nitride (Si3n4) Nanopharaic Material

The silicon nitride (Si3N4) ceramic material has the following characteristics: high temperature strength, high hardness, good abrasion resistance, excellent antioxidant resistance. In structural ceramic materials, the high temperature field is the most used in the foreground [10]. The nanomaterial refers to a superfine material that reaches nanoscale (10-9 m), which is generally 1 to 100 nm. At present, nano-ceramic materials are being widely used in a variety of high-tech fields, such as metallurgical, chemical, electronics, and national defense. To obtain high-performance silicon nitride ceramics, high-performance silicon nitride powder and sintering aid powder must be prepared.

In the 1990s, the researchers have synthesized ultrafined amorphous namide silicon powder by using laser method, plasma arc method, etc. They successfully prepared an oxide ceramic powder having a particle diameter of less than 20 nm using an advanced sol-gel method, which opened up a new way for the preparation of nitride-based ceramics [11]. However, ceramic superplastic forming techniques are not mature, especially the superplastic forming law of ceramic parts of complex shapes, is still to be studied in-depth study. Using numerical simulation methods to simulate the ceramic parts superplastic forming process is an effective means of obtaining superplastic forming regularities while reducing experiments and production costs.

3.2. Application of Computer Aided in Chemical Industry

In recent years, with the rapid development of information technology and the application of artificial intelligence technology in many fields, many scholars are committed to introducing computer technology into the design of the chemical industry, and has made certain progress [12]. Scientists introduced some realistic cases of industrial design of computer-aided catalysts, which constructs a model of information data such as a specific surface area, aperture structure, and other aspects of a catalyst. Then they optimized the model with a computer. This type of computer-assisted optimization method has achieved a certain effect on the development of catalyst formulations in oil refining, car exhaust gas purification, desulfurization. At present, artificial neural network, intelligent optimization algorithm is a hot application method in computer assisting methods in the field of chemical industry.

Scientists describe the artificial neural network similar to simplifying the "black box" model of the human brain and the biological neurons of the natural nervous system. The connection model composed of neuronal and weight is a typical artificial neural network form, which is shown in Figure 1.

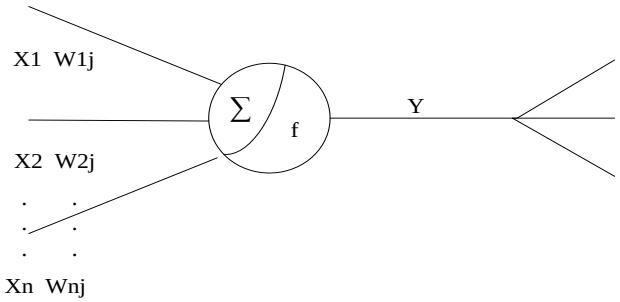

Figure 1. Artificial neuron model

In general, the input layer, the hidden layer, and the output layer are an indispensable part of

artificial neural network. The input vector can be represented by $x=(x1,x2,...,xn)$, and $x_n(n=1,n=2,...,n=n)$ is the nth input of the neuron in the formula. N is the number of input neurons, the function intensity between the neurons n and j is represented by weight w_{nj} . θ is a threshold of neurons, then input weighting and A are:

$$a=\sum_{n=1}^{n} x_n w_{nj}-\theta \tag{1}$$

The output of neurons is: y = f (a), the function f (a) is a transfer function between the neural networks different layers. It has been widely accepted for methods, optimization, classification, prediction, and decision-making methods for various fields. The following types are common intelligent optimization algorithms:

(1) Genetic algorithm

Theoretical foundation of GeneticalgorithiMs, GA is the genetic principle and natural selection of biological. It uses group search skills to select a series of genetic operations such as current groups, intersecting, and variability, such as a new generation of groups, which gradually enables groups to include or approximate the optimal solution to improve their algorithm efficiency. The step diagram of the genetic algorithm is shown in Figure 2. The genetic algorithm shows that the universal framework of complex system optimization is not dependent on the problem itself. It has strong robustness to the problem, so it has a wide range of scientific.

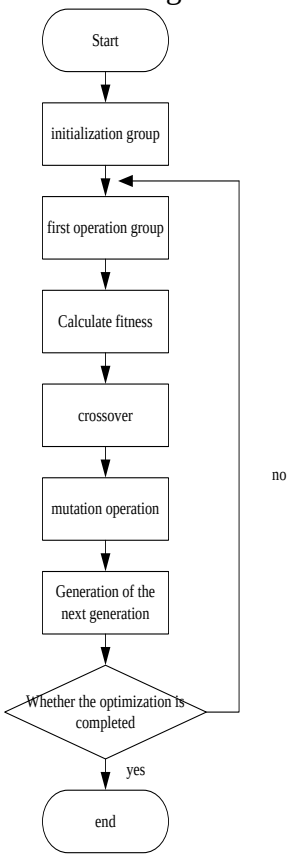

Figure 2. Procedure of the genetic algorithm

(2) Ant colony algorithm

The ACO algorithm is an intelligent optimization algorithm developed from the inspiration of

the ant individuals in order to forag. The search process of the ant colony algorithm is not from a certain point but from multiple points, it essentially belongs to a parallel optimization algorithm [13]. It has many advantages, such as strong robustness, better stability, and no excessive requirements for the selection of population initial paths. And its parameter setting is simple, easy to operate, only a slight modification can be applied to the residual optimization problem.

(3) Artificial fish group algorithm

The artificial fish group algorithm is an intelligent optimization algorithm for inspiration from the four basic behaviors of the fish group in nature [14]. The principle is to build a virtual artificial fish, the surrounding environment for visual stimulation for virtual artificial fish, forcing the virtual artificial fish to make corresponding behavior choices, gather swimming to places with higher food concentrations in the waters. Three main behaviors of artificial fish formation: Foraging behavior is virtual artificial and fish with a perceptual organ, feel the act of aggregation of the surrounding environment or high food concentration, this behavior is the basis of the convergence of artificial fish group algorithm; the clustering behavior is the behavior of the tendency of the virtual artificial fish with the direction of the same class near the vicinity, which allows the algorithm to have better stability. Rear-end behavior is the case where the virtual artificial fish is more active to the peripheral fish, this behavior is beneficial to the convergence rate of the algorithm and the globality of the reinforcing algorithm [15].

The ANN model is used to predict the adsorption efficiency (dye removal percentage) and adsorption capacity (load amount) on the surface of TiO2 on the surface of TiO2. It uses three input parameters training ANN models, such as pH, TiO2 dosage and initial dye concentration, and find the best quantity of neurons in the hidden layer by repeated testing.

3.3. Silicon Nitride Ceramic Material Process Operation and Results

The amorphous nano-Si3N4 ceramic powder is indeed an amorphous nanofin. The fine particles are small and uniform, with an average grain diameter of 18 nm, and has a high specific surface area and an oxygen-containing amount [16].

The art is a common method of preparing ceramic materials and nanomaterials, one of the main methods of sintering the preparation of a nitride-based ceramic material. Figure 3 is a schematic illustration of different stages of liquid phase sintering, Table 1 is the type of reaction liquid phase sintering.

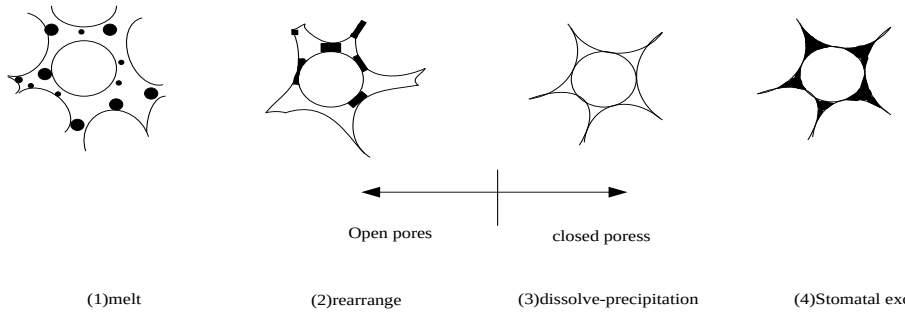

Figure 3. Schematic diagram of different stages of liquid phase sintering

Basic requirements for LPS sintering process: (1) There must be a liquid phase in the material sintering temperature range; (2) The solid phase can be infiltrated by the liquid phase material (ie, low contact angle); (3) The solubility of the solid phase in the liquid phase can meet the requirements. During the LPS sintering process, the densification of the material is three obvious stages, namely the rearrangement stage, the dissolution-precipitation phase, and the air hole

discharge stage.

Table 1. Types of the reaction night combination structure

Stage	Reaction	Example
1	A(s)+b(s)→a+liquid phase	Al_2o_3;si_3n_4+mgo
2	A(s)+b(s)+c(s)→a+ β +liquid phase	Sic+al_4c_3 +al_2o_3
3	A(s)+b(1)→a	Excess liquid phase
4	A(s)+b(s)→a_xb_y+liquid phase	Ba tio_3,pzt

Due to the easy decomposition characteristics of Si3N4 ceramics, liquid phase sintering is the only practical method that can cause the sintered block material [17]. The preparation method of the tensile sample is the same as the material sintering method. The sample sintering mold is designed and manufactured separately, and the tensile test is carried out in the hot press sintering furnace. Before the tensile test, each portion was installed in order, and in a vacuum hot press, the tensile deformation of the sample was achieved by loading the press.

4. Based on Computer-assisted Tang Sangcai Crafts Surface Nano-processing Technology

4.1. Optimizing the Process Conditions of Nano-silicon Nitride (Si3n4) Based on Computer Aids

As the catalyst using CaO, nanosine oxidation was carried out using acetonitrile as a solvent and H2O2 (30%) as an oxidant [18]. This experiment takes into account the effects of reaction temperature, reaction time, catalyst, solvent dosage and oxidant dosage on product yield. The reaction was carried out under vigorous stirring (600 rpm). The yield of the product can be calculated from the nitride conversion and product selectivity [19]. Because the artificial neural network is far better than analog prediction outside the application domain [20], the distribution of sample data in the super plane of the process optimization model should be as uniform, so that it can better represent the initial samples. It is possible to ensure that the ability to process conditions is very large and will not miss the best process conditions.

Based on the above, the use of random prepared process conditions, as an initial sample, it is clearly to increase the difficulty of the preferred process, and it is difficult to ensure better process conditions [21]. After setting the range of each process condition, it has good uniformity and good performance by orthogonal design methods. Therefore, it is necessary to design the initial sample by orthogonal design method. By preparing 15 initial samples, normalized between [0, 1]. Data samples are shown in Table 2.

(1) GRNN model structure optimized for process conditions

The GRNN algorithm has a wide range of applications in the field of prediction and control [22]. The pre-processing of the data set is a key step in the GRNN prediction process. Fitting, omitting anomalous value, identifying lost data, etc. is a common method of data pretreatment. Flexible network structure and good robustness are two major advantages of GRNN handling nonlinear problems. GRNN is a probability function network that consists of a four-layer network structure of GRNN, an analog layer, a sum: layer, and an output layer. The evaluation layer calculating the probability density function is a neuron with more output layers. The function of other neurons is to calculate the output. GRNN is more advantageous when running than other iterative training networks, so it is more effective [23]. Figure 4 is a structure of a GRNN model used in the text.

Table 2. 60 ℃ Types of reactive night combination structure

No	Timeh(x_2)	The amount of catalyst G(x_3)	Solvent dosage Ml(x_4)	Oxidant dosage Ml(x_5)	Yield(y_1)
1	1	0.05	4.2	2.45	0.9366
2	2	0.06	4.2	2.45	0.5089
3	3	0.06	4.2	2.45	0.6901
4	4	0.06	4.2	2.45	0.7848
5	5	0.06	4.2	2.45	0.8668
6	6	0.06	4.2	2.45	0.9028
7	7	0.06	4.2	2.45	0.9103
8	8	0.06	4.2	2.45	0.9243
9	9	0.06	4.2	2.45	0.9332
10	10	0.06	4.2	2.45	0.9386
11	10	0.07	4.2	2.45	0.9308
12	10	0.06	4..2	3.69	0.4667
13	10	0.06	2.1	2.45	0.7909
14	10	0.06	3.1	2.45	0.8399
15	10	0.06	5.2	2.45	0.5364

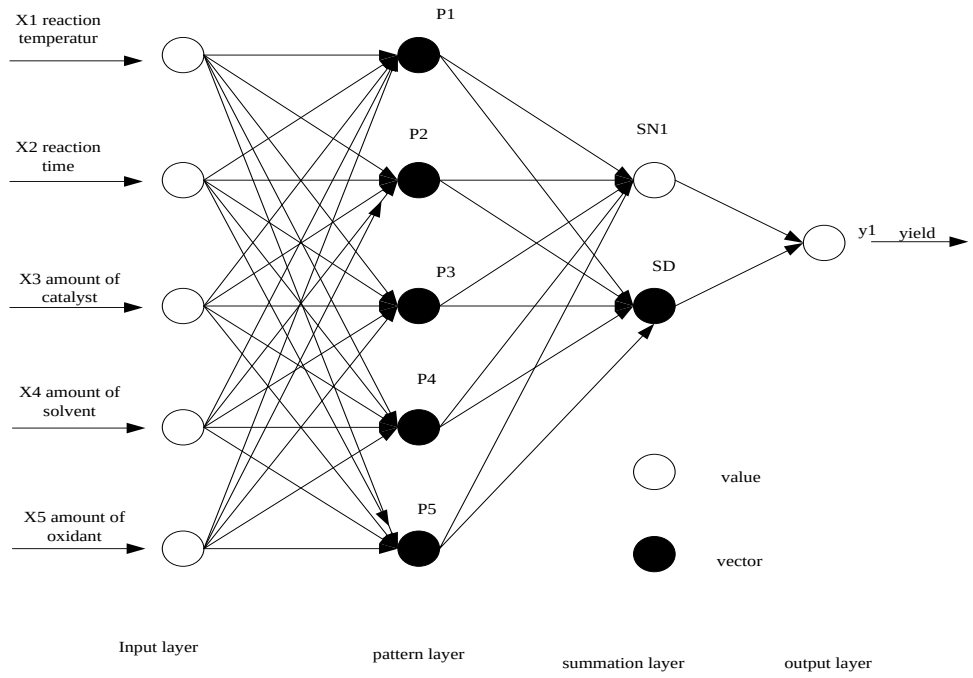

Figure 4. GRNN model structure

Nonlinear regression is the theoretical basis of GRNN, and Y calculates the regression analysis based on the self-variable X and the corresponding argument y. The condition mean is equation:

$$\overset{\Lambda}{Y} = E(y/X) = \frac{\int_{-\infty}^{\infty} yf(X,y)dy}{\int_{-\infty}^{\infty} f(X,y)dy} \quad (2)$$

Wherein F (x, y) is the probability density function, X is the measured value of X, Y is the predicted output of Y under the condition of input X. Using PARZEN non-parameter estimation, $\hat{f}(x,y)$ can be estimated from sample data $\{x_i, y_i\}_{i=1}^{n}$.

$$\hat{f}(X,y)=\frac{1}{n(2\pi)^{\frac{p+1}{2}}\sigma^{p+1}}\sum_{i=1}^{n}\exp\left[-\frac{(X-X_i)^T(X-X_i)}{2\sigma^2}\right]\exp\left[\frac{(X-Y_i)^2}{2\sigma^2}\right] \tag{3}$$

Where x_i is the measurement of X, y_i 2 is Y's measurement; N is the sample amount; P is the dimension of x; the σ, called smoothing factor is the width coefficient of the Gaussian function.

$\hat{f}(x,y)$ replace to $\hat{Y}$, and exchange the order of adding and adding:

$$\hat{Y}(X)=\frac{\sum_{i=1}^{n}\exp\left[-\frac{(X-X_i)^T(X-X_i)}{2\sigma^2}\right]\int_{-\infty}^{\infty}y\exp\left[-\frac{(Y-Y_i)^2}{2\sigma^2}\right]dy}{\sum_{i=1}^{n}\exp\left[-\frac{(X-X_i)^T(X-X_i)}{2\sigma^2}\right]\int_{-\infty}^{\infty}\exp\left[-\frac{(Y-Y_i)^2}{2\sigma^2}\right]dy} \tag{4}$$

Therefore, $\int_{-\infty}^{\infty}ze^{-z^2}dz=0$, two points can be obtained, and then the output of the network is:

$$\hat{Y}(X)=\frac{\sum_{i=1}^{n}Y_i\exp\left[-\frac{(X-X_i)^T(X-X_i)}{2\sigma^2}\right]\int_{-\infty}^{\infty}y\exp\left[-\frac{(Y-Y_i)^2}{2\sigma^2}\right]dy}{\sum_{i=1}^{n}\exp\left[-\frac{(X-X_i)^T(X-X_i)}{2\sigma^2}\right]\int_{-\infty}^{\infty}\exp\left[-\frac{(Y-Y_i)^2}{2\sigma^2}\right]dy} \tag{5}$$

The estimated value $\hat{Y}(X)$ is the weighted average of all measurement y_i, and the weighting factor of each y_i is the square of the equivalent of the corresponding sample X_i and X, the following steps below the step of the grunn network:

Step 1: Initializing the input neuron input layer: X1 reaction temperature, X2 reaction time, X3 catalytic dose, X4 solvent amount and X5 oxidizing dose, which is a factor affecting product yield.

Step 2: Calculate the analog neurons. The number of neurons in the mode layer is equal to the number of learning samples. It sets the weight to 1 and allows input index vectors to pass to each neuron mode. It uses the radial basis function to calculate the output of each mode neuron:

$$p_i=\exp\left[-\frac{(X-X_i)^T(X-X_i)}{2\sigma^2}\right]i=1,2,3,4,5 \tag{6}$$

Step 3: Calculate and neuron. Summarize two types of neurons in the layer. A class of formulas is:

$$\sum_{i=1}^{n}\exp\left[-\frac{(X-X_i)^T(X-X_i)}{2\sigma^2}\right] \tag{7}$$

It is the summary of all analog layers, analog layers and neuron connection weights are 1, and

the transfer function is:

$$S_D = \sum_{i=1}^{n} p_i \tag{8}$$

Another type of formula is:

$$\sum_{i=1}^{n} Y_i \exp\left[-\frac{(X - X_i)^T (X - X_i)}{2\sigma^2} \right] \tag{9}$$

It is the weighted sum of all analog layers output. The i-th neurons in the simulation layer are added to the jinary molecules in the summary layer. The connection weight between the neurons is the J20 of the i-i output sample y_i. The transfer function is:

$$S_{Nj} = \sum_{i=1}^{n} y_i p_i (j = 1,2,...,k) \tag{10}$$

Step 4: The output value of the yield SNJ is divided by the output value of SD. The predicted yield can be obtained by the following equation:

$$y_j = \frac{S_{Nj}}{S_D} (j = 1,2,...,k) \tag{11}$$

Setting the smoothing parameter "σ" is manually done throughout the modeling process. The setting of smoothing parameters has an important impact on the generalization capacity and prediction accuracy of GRNN. The following chapters will discuss the optimization of "σ" [24].

(2) Improved GRNN network modeling

1. Determine the variable affecting the product production and record the original data in the experiment.

2. Normalize the input data to between 0 and 1.

$$y = (x \bullet x_{\min})(x_{\min} \bullet x_{\max}) \tag{12}$$

Where Y is a normalized value of x_i. $x_{\max}$ is the maximum value of x_i, $x_{\min}$ is the minimum of x_i. The standardization of input data increases the training rate of the network.

3. Raise the collected data into two groups of data. A group is training data for training networks, and another group is test data for verifying the network.

4. Build a network and use CV to optimize the model.

5. Select the best model based on the mean square error MSE.

$$MSE = \frac{1}{N} \sum_{i=1}^{N} (\left| y_{prd,i} - y_{\exp,j} \right|)^2 \tag{13}$$

Where N is the number of data, ^{prd,i} is the attribute feature of the i-th predicted, and ^{prd,i} is the i-th measurement. After establishing an improved GRNN model, the yield of the product can be described as a "function" of process conditions:

$$Y_{yield} = f(X_i) \tag{14}$$

The i represents the reaction temperature, reaction time, catalyst, solvent, and oxidizing dose. Figure 5 shows the steps of improved GRNN training processes for process conditions optimization:

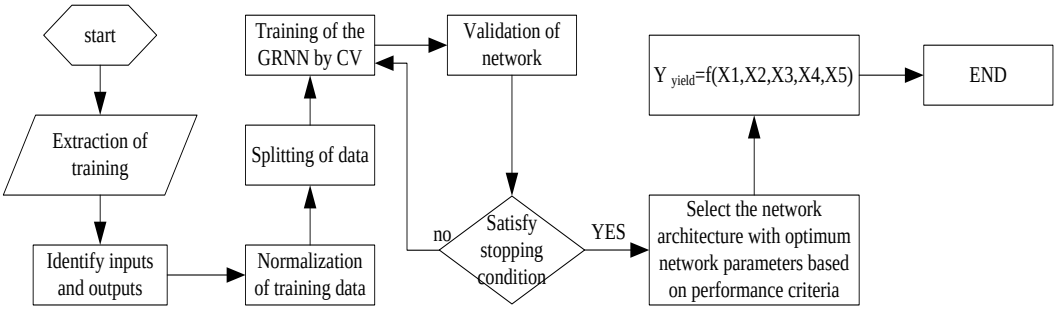

Figure 5. Improved GRNN training process for process conditions optimization

The optimal problem is that the main problems after modifying process operating conditions for improved GRNN, which can be expressed:

$$\max(Y_{yield}) = f(X_i), s.t. X_{\min} \leq X_i \leq X_{\max} \quad (15)$$

The above equations are constrained optimization problems, and the target function is a non-linear network, and the derivative is difficult to calculate, so it is difficult to solve it by analysis.

4.2. Improved GRNN Model Results and Discussion

The simulation is performed by MATLAB R2014A. First, MATLAB uses a function to construct a GRNN model [25]. The best smoothing parameters are selected according to the minimum cross-validation error from the training sample. Based on the number of samples of 15, the last 3 sets of data is used as the test sample. The parameter k in the cross-validation is obtained according to the formula. In order to select an optimum value, by using a method of cyclic training. [0.1, 2] is considered an initial search interval for optimal values. Table 3 shows the best minimum MSE of each of the seven cross-validation results.

Table 3. Minimum σ of each of the seven cross-validation results MSE

Frequency	Σ	Mse
1	1	0.0073665
2	2	0.029554
3	0.1	0.0085271
4	0.2	0.0014548
5	0.1	0.0019757
6	2	0.089216
7	0.1	0.0010223

As can be seen from the results, the smaller the σ value, the stronger the approximation of the

sample; the larger the MSE value, the smoother the process of approaching the sample data, but the error will increase accordingly [26]. Obviously, the seventh cross-validation is the best. Therefore, the input seventh cross-verification is used as the optimal input, and the output is used as the optimal output to establish an improved GRNN model.

The program operation results show that the established model MSE is 0. 0029979. As can be seen from Figure 6, the model prediction results are very close to the experimental results, and the improved GRNN is described, especially several low-yield samples can also be well simulated. The assessment of the performance of the trained neural network not only depends on its training accuracy, but also depends on its generalization accuracy, that is, its generalization performance [27]. Therefore, only two aspects have reached a certain accuracy to say that the network performance is good. Figure 6 shows the last three sets of data prediction errors that are not covered in the training model. It can be clearly seen from Figure 6 that all prediction errors of three samples of the improved GRNN are within 0.05. In addition, GRNN and BPNN were used as comparative models. The test results show that the improved GRNN model has good correlation with the experimental data and has good predictive capabilities. Therefore, the model construct is successful. A function obtained by Y = F (Xi), and i represents the reaction temperature, reaction time, catalyst amount, solvate, and oxidizing dose.

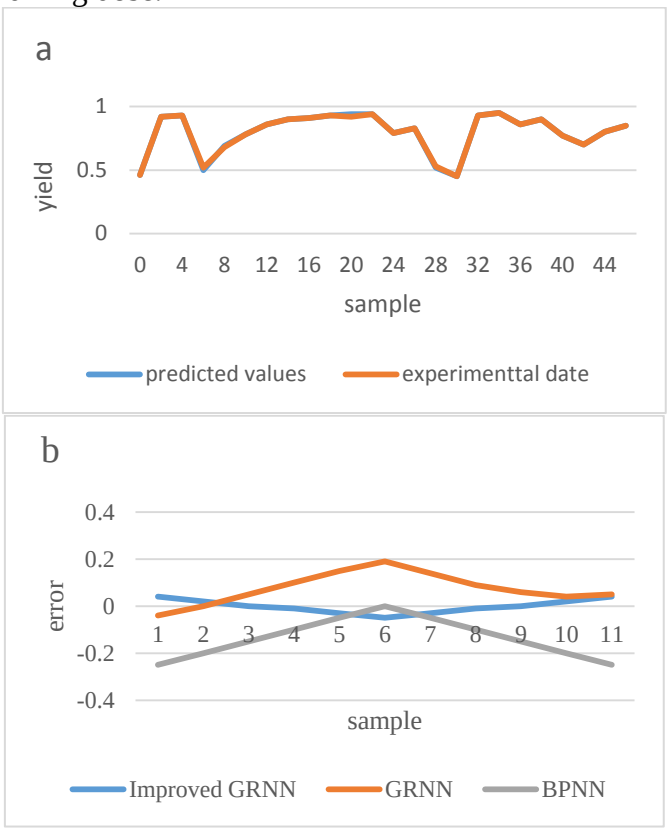

Figure 6. Comparison of improved GRNN prediction accuracy and GRNN prediction error

When the sample data is less, the improved GRNN is better. Therefore, it can extend to other multi-process or complex processes of industrial product prediction modeling and optimization applications [28].

4.3. Si2N2O-Si3N4 Ceramic Superplastic Drawing and Simulation

The Y2O3 and Al2O3 nano-ceramic powder prepared by amorphous nano-Si3N4 ceramic

powder, a polymer network gel method were mixed in a mass ratio, and the ball mill was grinded with a ball mill. The slurry is then dried and ground, sintering in a vacuum hot press furnace. The sintering temperature was 1600 ℃, the pressure was 30 MPa, and the nitrogen pressure was 0.1MPa; the sintered block was 30 mm, the thickness was 1 mm.

The composition and microstructure of the sintered block body is shown in Figure 7, the sintering body is mainly composed of β-Si3N4 and Si2N2O, and the particle diameter is less than 280 nm [41, 42].

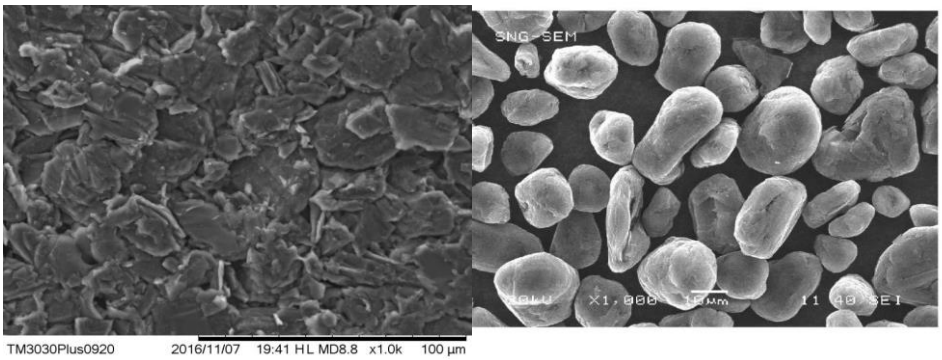

Figure 7. Microstructure of sintered body

By drawing the test, the ceramic superplasticity is studied, the mold is shown in Figure 8. The ceramic sheet is obtained by hot press sintering, with a diameter of 30 mm and a thickness of 1 mm. When forming, the sheet is simultaneously placed in a sintering apparatus, and a boron nitride powder is added between the convex mold and the pressure side to increase the pressure brake during the forming process. The test pulsed deep shaped temperature was 0.1 mm / min, 0.2 mm / min, 0.5 mm / min, respectively. Table 4 is the result of the measurement of ceramic forming body under different conditions, respectively.

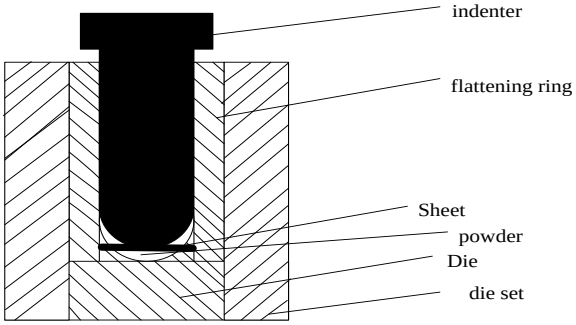

Figure 8. Schematic diagram of superplastic forming mold

Table 4. Ceramic shaped body measurement results

deformation rate (mm/min)	thickness(mm)				Radius reduction (mm)
	A point	B point	C point	D point	
0.1	0.52	0.72	0.8	0.79	1.4
0.2	0.6	0.78	0.8	0.8	0.8
0.5	0.61	0.82	0.8	0.81	0.5

The rigid plastic model of the ceramic material superplastic deformation can be approximately:

$$\sigma = K \dot{\varepsilon}^{m} \tag{16}$$

The constant related to the material in the formula; $\dot{\varepsilon}^{m}$ strain rate (s^{-1}); m strain rate sensitivity index.

The secondary development of ANSYS software was carried out, and the model used the GRNN model to simulate the Si2N2O-Si3N4 ceramic material superplastic derrown process. The three-dimensional finite element entity model and the formation result are shown in Figure 8 is set to the non-deformed body. Their inner diameter is 20mm, the convex mode is fixed, the recess is fixed, and the rounded radius is 1.5 mm. Friction between the mold and the sheet is a shear friction model, ie F = MT. In the formula m is the friction factor, it is set to 0.3 according to the friction conditions, and T is the pressure brake.

The stress strain curve obtained by the Si2N2O-Si3N4 ceramic obtained by tensile test is shown in Figure 9. As can be seen from the figure, the elongation of Si2N2O-Si3N4 ceramics at 1550 °C can reach 65%, the stress is less than 20 MPa, and the curve of different temperatures is extracted during the simulation process.

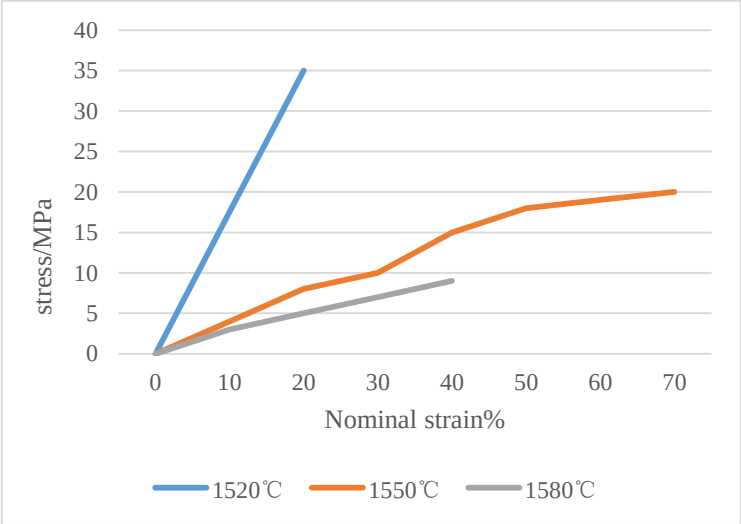

Figure 9. Total stress strain curve of Si2N2O-SIN4 at different temperatures

Since the molding temperature is high, the mold material is high in graphite, so the mold design is relatively simple. The pressure brake is mainly obtained by adding the friction between the powder and the crimp ring and the outer sleeve, and the value of the pressure brake is small, and the secondary force is 0.2K in the simulation process. As the forming process progresses, the radius of the ceramic plate is gradually contracted, which is consistent with the test results. Figure 10 shows the simulation result of the radius decrease with the interval change when the radius is given. As can be seen from Fig. 10, the shrinkage value of the ceramic body radius is reduced as the formation rate increases. This is mainly due to the fact that the ceramic body is thinner, resulting in a reduction in the amount of outer diameter shrinkage deformation, which is consistent with the volume constant principle in the process of plastic deformation. As the forming process a progress, the crown portion is gradually thinned, and the radial contraction capacity is lowered, so the shrinkage rate is reduced. Compared with the test results, when the formation rate is 0.1 mm / min, the error is large, and the error is 10%; when the formation rate is 0.2 mm / min and 0.5 mm / min, the error is small, less than 5%. This is mainly due to the low-shaped rate, due to the long time of the material, it is difficult to maintain the deformation performance.

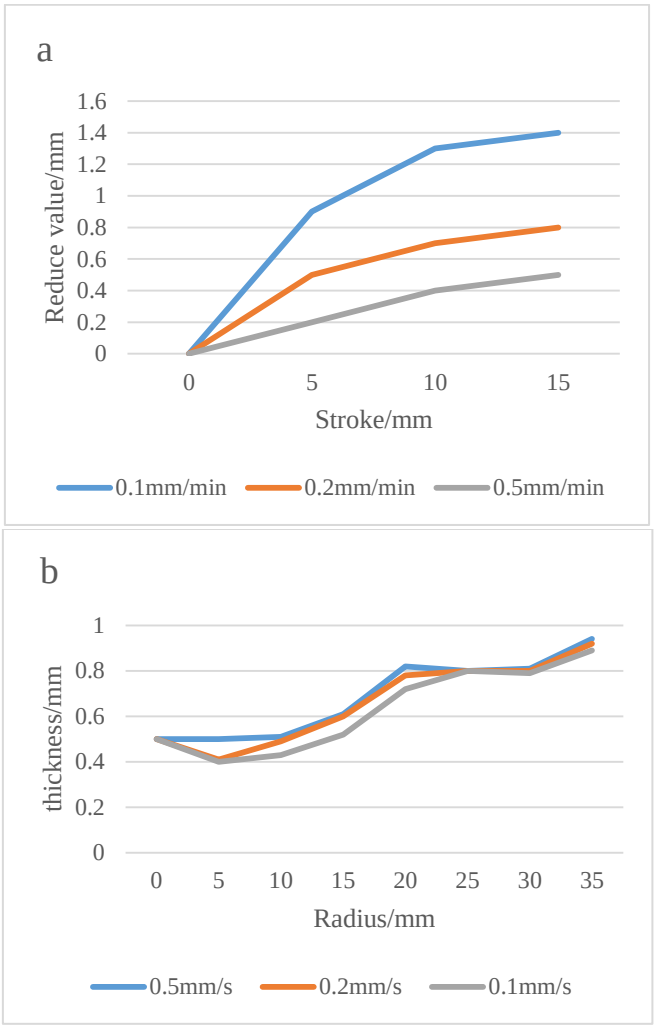

Figure 10. Decrease amount and different forming rate of different forming rates in the radius of the ceramic body

The simulation results of different forming rate shaped parts are shown in the radius direction, as shown in Figure 10, it can be seen: The wall thickness of the shaped part is distributed between 0.35-0.95mm, and the maximum thin point of the molded body is not located in the vertex of the molded body, but is adjacent to the vertex. As the formation rate is improved, the molded body is thinned and consistent with the experimental results. However, during the actual forming process, the forming rate is too low, the time required for the forming is increased, and the grains grow up quickly when the material is high, and the molding capability of the test piece will also be reduced.

5. Discussion

Silicon nitride (Si3N4) oxidation reaction process operating conditions, using an improved GRNN model to simulate functional relationship between silicon oxide conditions and product yields. It is then experimentally experiment with the optimal process conditions obtained by model optimization, and the experimental data is measured and compared with the model prediction, find the relationship between the reaction temperature, the reaction time, the catalyst amount, the amount of solvate, and the oxidizing dose.

Silicon nitride ceramic materials are a high-temperature ceramic material that is mostly used in

the field of application in the field. The article was sintered with a hot pressure sintering process liquid phase sintered amorphous nano-Si3N4 powder, and Si2N2O-Si3N4 and Si2N2O-Sialon nanophara was prepared. It combined with finite element simulations by experimental study, the basic laws of superplastic forming of two ceramic materials were studied.

6. Conclusion

Through the silicon nitride ceramic block material, the low temperature superplastic forming of silicon nitride ceramics is achieved, and the basic law of silicon nitride ceramic superplasticity is obtained. The shrinkage value of the outer diameter of the ceramic body increases with the reduction rate of the forming rate, and the shrinkage rate will gradually decrease with the formation process. The maximum thinning point of the molded body is not in the vertex of the molded body, but is a ring region near the vertex. As the formation rate is improved, the molded body is thinned. These regularities have reference value and guiding significance for the control of the wall thickness of ceramic products.

Funding

This article is not supported by any foundation.

Data Availability

Data sharing is not applicable to this article as no new data were created or analysed in this study.

Conflict of Interest

The author states that this article has no conflict of interest.

Reference

[1] Anitha R, Raja D. Development of computer‐aided approach for brain tumor detection using random forest classifier. International Journal of Imaging Systems & Technology. (2018) 28(1): 48-53. https://doi.org/10.1002/ima.22255

[2] Acharya V, Kumar P. Identification and red blood cell automated counting from blood smear images using computer-aided system. Medical & Biological Engineering & Computing. (2018) 56(16): 483-489. https://doi.org/10.1007/s11517-017-1708-9

[3] Bukhari N I, Julianto T, Pereira R. Computer-aided prediction of cefotaxime sodium stability in aqueous solution at different pH from sparse data. Latin American Journal of Pharmacy. (2018) 37(3): 571-578.

[4] Daemei A B, Safari H. Factors affecting creativity in the architectural education process based on computer-aided design. Frontiers of Architectural Research. (2018) 7(1): 100-106. https://doi.org/10.1016/j.foar.2017.09.001

[5] Alanis, Alma Y. Electricity Prices Forecasting using Artificial Neural Networks. IEEE Latin America Transactions. (2018) 16(1): 105-111. https://doi.org/10.1109/TLA.2018.8291461

[6] Ravichandran V, Li C, Banagozar A. Artificial neural networks based on memristive devices. Science China Information Sciences. (2018) 61(6): 1-14. https://doi.org/10.1007/s11432-018-9425-1

[7] Dc A, Rm B, Lz A. Characterizing the chemical composition of Tang Sancai wares from five Tang dynasty kiln sites. Ceramics International. (2020) 46(4): 4778-4785. https://doi.org/10.1016/j.ceramint.2019.10.210

[8] Widerski A, Arkadiusz Jówiak, Jachimowski R. Operational quality measures of vehicles applied for the transport services evaluation using artificial neural networks. Eksploatacja i Niezawodnosc - Maintenance and Reliability. (2018) 20(2): 292-299. https://doi.org/10.17531/ein.2018.2.16

[9] Zhang L, Zhou J, Yang J. Study of the Synergistic Effect of Hydrogen Bonding and Nano-Si3N4 in XNBR Matrix. Journal of Inorganic and Organometallic Polymers and Materials. (2021) 31(7): 2859-2867. https://doi.org/10.1007/s10904-021-01972-9

[10] D P S J K P, Ruby J. Computer Aided Therapeutic of Alzheimer's Disease Eulogizing Pattern Classification and Deep Learning Protruded on Tree-based Learning Method. Advances in Intelligent Systems and Computing. (2018) 564(1): 103-113. https://doi.org/10.1007/978-981-10-6875-1_11

[11] Suto J, Oniga S. Efficiency investigation of artificial neural networks in human activity recognition. Journal of Ambient Intelligence & Humanized Computing. (2018) 9(4): 1-12. https://doi.org/10.1007/s12652-017-0513-5

[12] Alomari M H, Adeeb J, Younis O. Solar Photovoltaic Power Forecasting in Jordan using Artificial Neural Networks. International Journal of Electrical and Computer Engineering. (2018) 8(1): 497-504. https://doi.org/10.11591/ijece.v8i1.pp497-504

[13] Mundada V, Suresh K. Optimization of Milling Operations Using Artificial Neural Networks (ANN) and Simulated Annealing Algorithm (SAA). Materials today: proceedings. (2018) 5(2): 4971-4985. https://doi.org/10.1016/j.matpr.2017.12.075

[14] Czischek S, Gaerttner M, Gasenzer T. Quenches near Ising quantum criticality as a challenge for artificial neural networks. Physical review. B, Condensed Matter and Materals Physics. (2018) 98(2): 024311.1-024311.10. https://doi.org/10.1103/PhysRevB.98.024311

[15] Rahmanadi L, Sulistiyono H. Hybrid technique between design of experiments and artificial neural networks for rainfall-runoff model calibration method. International Journal of Civil Engineering and Technology. (2018) 9(1): 11-21.

[16] Goay C H, Goh P, Ahmad N S. Eye-height/width prediction using artificial neural networks from S-Parameters with vector fitting. Journal of Engineering Science and Technology. (2018) 13(3): 625-639.

[17] Saha G, Chakraborty K, Das P. Voltage Stability Prediction on Power Networks using Artificial Neural Networks. Indonesian Journal of Electrical Engineering and Computer Science. (2018) 10(1): 1-9. https://doi.org/10.11591/ijeecs.v10.i1.pp1-9

[18] Miona, V, Andrejevi. Implementation of Recurrent Artificial Neural Networks for Nonlinear Dynamic Modeling in Biomedical Applications. The International Journal of Artificial Organs. (2018) 36(11): 833-842. https://doi.org/10.5301/ijao.5000255

[19] Charfi S, Ansari M E. Computer-aided diagnosis system for colon abnormalities detection in wireless capsule endoscopy images. Multimedia Tools and Applications. (2018) 77(3): 4047-4064. https://doi.org/10.1007/s11042-017-4555-7

[20] Qin Y, Lu W, Qi Q. Towards an ontology-supported case-based reasoning approach for computer-aided tolerance specification. Knowledge-Based Systems. (2018) 141(2)129-147. https://doi.org/10.1016/j.knosys.2017.11.013

[21] Nguyen P T, Huynh V, Vo K D. An Optimal Deep Learning based Computer-aided Diagnosis System for Diabetic Retinopathy. Computers, Materials and Continua. (2021) 66(3): 2815-2830. https://doi.org/10.32604/cmc.2021.012315

[22] Aldegheishem A. Computer-Aided-Design and Manufacturing of Full Mouth Restoration of a Male Patient with Gastroesophageal Reflux Disease: A Case Report. Bioscience Biotechnology Research Communications. (2021) 14(1): 100-104. https://doi.org/10.21786/bbrc/14.1/13

[23] Saeed F, Rashid A, Saleem W. Implications of Computer-Aided Learning in Elt for Second Language Learners and Teachers During Covid-19. Humanities & Social Sciences Reviews. (2021) 9(3): 1528-1541. https://doi.org/10.18510/hssr.2021.93154

[24] Ma K N, Chen H, Ye H Q. Advances in computer aided design and computer aided manufacturing of removable partial denture. Zhonghua kou qiang yi xue za zhi = Zhonghua kouqiang yixue zazhi = Chinese journal of stomatology. (2021) 56(5): 485-490.

[25] Li H, Zhang H, Zhao Y. Design of Computer-aided Teaching Network Management System for College Physical Education. Computer-Aided Design and Applications. (2021) 18(S4): 152-162. https://doi.org/10.14733/cadaps.2021.S4.152-162

[26] Wojnarowska W, Kwolek M, Miechowicz S. Selection of a workpiece clamping system for computer-aided subtractive manufacturing of geometrically complex medical models. Open Engineering. (2021) 11(1): 239-248. https://doi.org/10.1515/eng-2021-0026

[27] Wu H. Multimedia Interaction-Based Computer-Aided Translation Technology in Applied English Teaching. Mobile Information Systems. (2021) 2021(5): 1-10. https://doi.org/10.1155/2021/5578476

[28] Dc A, Rm B, Jc B. Circulation of Tang Sancai wares and lead materials in the two capital cities of the Tang empire. Ceramics International. (2021) 47(7): 10147-10152. https://doi.org/10.1016/j.ceramint.2020.12.163